The ENSO-Asian monsoon interaction in a coupled ocean-atmosphere GCM

The ENSO–Asian Monsoon Interaction in a Coupled Ocean–Atmosphere GCM

YING LI

CMSR, Institute of Atmospheric Physics, and Graduate School, Chinese Academy of Sciences, Beijing, China

RIYU LU

LASG, and CMSR, Institute of Atmospheric Physics, Chinese Academy of Sciences, Beijing, China

BUWEN DONG

Walker Institute for Climate System Research, University of Reading, and National Centre for Atmospheric Science-Climate, Reading, United Kingdom

(Manuscript received 31 May 2006, in final form 12 December 2006)

ABSTRACT

In this study, the authors evaluate the (El Niño–Southern Oscillation) ENSO–Asian monsoon interaction in a version of the Hadley Centre coupled ocean–atmosphere general circulation model (CGCM) known as HadCM3. The main focus is on two evolving anomalous anticyclones: one located over the south Indian Ocean (SIO) and the other over the western North Pacific (WNP). These two anomalous anticyclones are closely related to the developing and decaying phases of the ENSO and play a crucial role in linking the Asian monsoon to ENSO. It is found that the HadCM3 can well simulate the main features of the evolution of both anomalous anticyclones and the related SST dipoles, in association with the different phases of the ENSO cycle.

By using the simulated results, the authors examine the relationship between the WNP/SIO anomalous anticyclones and the ENSO cycle, in particular the biennial component of the relationship. It is found that a strong El Niño event tends to be followed by a more rapid decay and is much more likely to become a La Niña event in the subsequent winter. The twin anomalous anticyclones in the western Pacific in the summer of a decaying El Niño are crucial for the transition from an El Niño into a La Niña. The El Niño (La Niña) events, especially the strong ones, strengthen significantly the correspondence between the SIO anticyclonic (cyclonic) anomaly in the preceding autumn and WNP anticyclonic (cyclonic) anomaly in the subsequent spring, and favor the persistence of the WNP anomaly from spring to summer. The present results suggest that both El Niño (La Niña) and the SIO/WNP anticyclonic (cyclonic) anomalies are closely tied with the tropospheric biennial oscillation (TBO). In addition, variability in the East Asian summer monsoon, which is dominated by the internal atmospheric variability, seems to be responsible for the appearance of the WNP anticyclonic anomaly through an upper-tropospheric meridional teleconnection pattern over the western and central Pacific.

1. Introduction

Coupled ocean–atmosphere general circulation models (CGCMs) are essential tools to study long-term climate variations and the effects of global warming. It is believed that the models' successful simulation of teleconnections in the present conditions would justify their prediction of the regional and global climate change. Therefore, the motivation of this study is to evaluate the interaction between the El Niño–Southern Oscillation (ENSO) and Asian monsoon in a CGCM, as well as to advance our understanding of this interaction.

The ENSO–Asian monsoon interaction is one of the most dominant coupled phenomena in the climate system and has long been a subject of scientific and practical interest. While both the ENSO variability and Asian monsoon variability are caused by the presence of ocean–atmosphere coupling, their interaction also

Corresponding author address: Riyu Lu, Institute of Atmospheric Physics, Chinese Academy of Sciences, P.O. Box 9804, Beijing 100029, China.
E-mail: lr@mail.iap.ac.cn

DOI: 10.1175/JCLI4289.1

occurs through an ocean–atmosphere coupled system. Kirtman and Shukla (2002) showed that without the air–sea coupling, the impact of the monsoon on the ENSO is absent, and it is difficult to capture the observed ENSO–monsoon relationship. Thus, capturing the observed ENSO–Asian monsoon coupling is one of prerequisites for a CGCM to depict reliable long-term climate variations and project changes of both Asian climate and ENSO in response to greenhouse gas forcing.

The interaction between the Asian monsoon and ENSO has been extensively studied in terms of the western North Pacific (WNP) monsoon, the East Asian monsoon, and the South Asian monsoon due to their distinctive characteristics (e.g., Lau et al. 2000; Wang et al. 2001). It has been found that climatic anomalies in the western North Pacific and East Asia sector (WNP/EA) are related to the different phases of ENSO (Wang et al. 2000; Wang and Zhang 2002; Lu 2002; Chou et al. 2003). In particular, the anomalous low-level anticyclone over the WNP plays an important role in the relationship between the ENSO and WNP/EA climate anomalies (Zhang et al. 1999; Chang et al. 2000; Lau and Nath 2000; Wang et al. 2000). On the other hand, the interaction between the South Asian monsoon and ENSO has been extensively studied (Rasmusson and Carpenter 1982; Shukla and Paolino 1983; Elliot and Angell 1987; Webster and Yang 1992; Prasad and Singh 1996; and many others). The Indian summer monsoon rainfall precedes the Southern Oscillation and is negatively correlated with SSTs in the eastern equatorial Pacific with the largest correlation occurring when the SSTs are lagging the rainfall by one to two seasons (Elliot and Angell 1987). This lead–lag relationship implies that the monsoon variability may affect the ENSO evolution, intensity, and periodicity (Chung and Nigam 1999).

Recently, Wang et al. (2003) revealed that the anomalous anticyclones over the WNP and the south Indian Ocean (SIO), which affect the climate over a broad Asian monsoon region, can be used to illustrate the interaction between the ENSO and the Asian monsoon. The WNP anomalous anticyclone forms in the boreal autumn of a developing El Niño, attains its peak amplitude in winter, and persists into the following spring and early summer, thus having a delayed impact on the climate in the WNP/EA (Wang et al. 2000). The SIO anomalous anticyclone, on the other hand, originates during the summer of a growing El Niño, rapidly reaches its peak intensity in the autumn, and decays when the El Niño matures. These anomalous anticyclones exhibit a seasonal evolution intimately related to developing and decaying phases of ENSO, with the SIO (WNP) anomalous anticyclones prior (subsequent) to the El Niño mature phase. Whether global fully coupled GCMs can simulate the two El Niño–associated evolving anticyclones and understanding their interaction with the ENSO cycle clearly need to be investigated.

On the other hand, the spectrum of the ENSO index shows a biennial peak in addition to the lower-frequency peak (Rasmusson et al. 1990; Barnett 1991), and the Asian monsoon also exhibits a behavior suggestive of the tropospheric biennial oscillation (TBO: Meehl 1994, 1997). For example, the interannual variability of both the Indian monsoonal rainfall and East Asian monsoonal rainfall exhibits a remarkable TBO feature: years with above-normal summer rainfall tend to be followed by ones with below-normal rainfall and vice versa (Yasunari 1990; Shen and Lau 1995). There are two distinct views on the cause of the TBO. One is that the atmosphere–ocean interaction in the Asian monsoon region alone can support the TBO (Li et al. 2006) and results in the biennial component of ENSO through the monsoon forcing (Kim and Lau 2001). The other view emphasizes the role of ENSO in triggering the TBO in the Asian monsoon region (Wang et al. 1999; Wang et al. 2000; Kug and Kang 2006).

Due to the fact that the ENSO–Asian monsoon interaction is attained essentially by atmosphere–ocean interaction and limited available observational data, the outputs by global atmosphere–ocean coupled GCMs can be valuable for a better understanding of the physical mechanisms responsible for the ENSO–Asian monsoon interaction if this interaction is simulated properly.

In this study, we mainly focus on the evolution of the SIO/WNP anomalous anticyclones and their relationship with the ENSO cycle, due to the crucial role of these circulation anomalies in linking the ENSO with the Asian monsoon. In particular, the biennial component of the relationship has been investigated. The model and the simulated climatology are described briefly in section 2. The coupling between ENSO and the Asian monsoon in this simulation is evaluated in section 3. The interaction between the SIO/WNP anomalous anticyclones and the ENSO cycle, and the relation between this interaction and TBO are analyzed in section 4. Section 5 contains a summary.

2. Model and its basic behavior

The model that we use is a version of the U.K. Hadley Centre CGCM, known as HadCM3 (Gordon et al. 2000). The atmospheric component of this model is run with a horizontal latitude–longitude grid spacing of

2.5° × 3.75° and 19 vertical levels using a hybrid vertical coordinate. A detailed description of the atmospheric model formulation and its performance in a simulation forced with observed SSTs is described in Pope et al. (2000). The oceanic component has 20 vertical levels with a 1.25° × 1.25° latitude–longitude grid. The vertical levels are distributed to provide enhanced resolution near the ocean surface. The two components are coupled once a day. Heat and water fluxes are conserved exactly in the transfer between their different grids. The coupled model uses preindustrial atmospheric trace gas concentrations, and incoming solar radiation provides the only external forcing. The model has been run without the use of flux adjustments for over 1000 years without appreciable drift in the model's climate (Gordon et al. 2000). In this study, we analyze the results in a 1000-yr integration of the model.

The model simulates well the amplitude of ENSO, as measured by the standard deviation of Niño-3 (5°S–5°N, 150°–90°W) SST anomalies (Collins et al. 2001), within the range of uncertainty of observations. The periodic nature of ENSO is also reproduced, with a broad spectral peak at 3–4 yr in the power spectrum of Niño-3 SST (Collins et al. 2001; AchutaRao and Sperber 2002). However, Collins et al. (2001) noted that the SST variability in the tropical Pacific in the model extends westward into the western Pacific warm pool. Despite this deficiency, HadCM3 has one of the most realistic representations of ENSO characteristics, including the amplitude, period, and phase locking with the seasonal cycle, among CGCMs (AchutaRao and Sperber 2002; Joseph and Nigam 2006). Although intercomparison studies of different CGCMs have shown that the model performance has improved over the years in representing ENSO-like behavior, only a few of these models are capable of reproducing the observed ENSO variability. In many models, simulated ENSO events are either too weak in amplitude or occur too frequently (e.g., Mechoso et al. 1995; Latif et al. 2001; Guilyardi 2006).

The observed data used in this study to evaluate model performance include the monthly precipitation data from 1979 to 2003 derived by the Climate Prediction Center (CPC) Merged Analysis of Precipitation (CMAP: Xie and Arkin 1997), reconstructed monthly mean SST from 1949 to 2003 (Smith and Reynolds 2004), and monthly mean National Centers for Environmental Prediction–National Center for Atmospheric Research (NCEP–NCAR) reanalysis data from 1949 to 2003 (Kalnay et al. 1996).

The basic state plays an important role for the ENSO–monsoon relationship (e.g., Turner et al. 2005). Thus, as a beginning, we briefly evaluate the model's ability to reproduce climatological features of the 850-mb wind and precipitation in the four seasons; see Fig. 1. The model simulates well the main features of the subtropical anticyclone over the western North Pacific, which forms in spring and strengthens in summer. In addition, the model reproduces the features of the anticyclonic circulation over the Indian Ocean, which appears in spring, intensifies, and extends farther northward in summer and retreats southward in autumn. The reversal of the mean Indian monsoonal flow from southwesterly in summer to northeasterly in winter is also captured. However, the simulated southeasterlies over the southern Indian Ocean appear to have a larger southern component than is observed throughout the four seasons.

Basic features of precipitation in the Tropics and subtropics are reasonably simulated. The model captures the main features of the intertropical convergence zone (ITCZ), which reaches the farthest north and is connected with the Asian monsoon region in boreal summer. The model reproduces the rainband over East Asia and the western Pacific and its seasonal migration. A rainband appears over south China and the western Pacific in spring, shifts northward in summer, retreats southward in autumn, and diminishes in winter. However, both the summer rainfall in East Asia and winter rainfall in the tropical southern Indian Ocean are too strong. The double ITCZ problem, noted by Mechoso et al. (1995), remains in this global coupled GCM without flux adjustment.

3. Evaluating the ENSO–Asian monsoon interaction in the model

Following AchutaRao and Sperber (2002) and Collins et al. (2001), we take the area-averaged SSTs in the Niño-3 region (5°S–5°N, 150°–90°W) as a simple measure of ENSO in the simulation. A warm (cold) event is defined when the Niño-3 index in a winter, December–February (DJF), is larger (less) than one standard deviation from the time mean. The standard deviation of DJF Niño-3 SST in the 1000-yr simulation is 0.96°C, slightly smaller than 1.05°C based on the observed SSTs from 1949 to 2003. This criterion yields 152 warm events and 156 cold events in the 1000-yr simulation. The winters corresponding to the selected ENSO events are designated as D(0)JF(1), and the years preceding and following these events are designated as Year (0) and Year (1), respectively.

Composite results based on the ENSO events in observations are shown in this section to facilitate evaluation of the simulated ENSO–Asian monsoon relation-

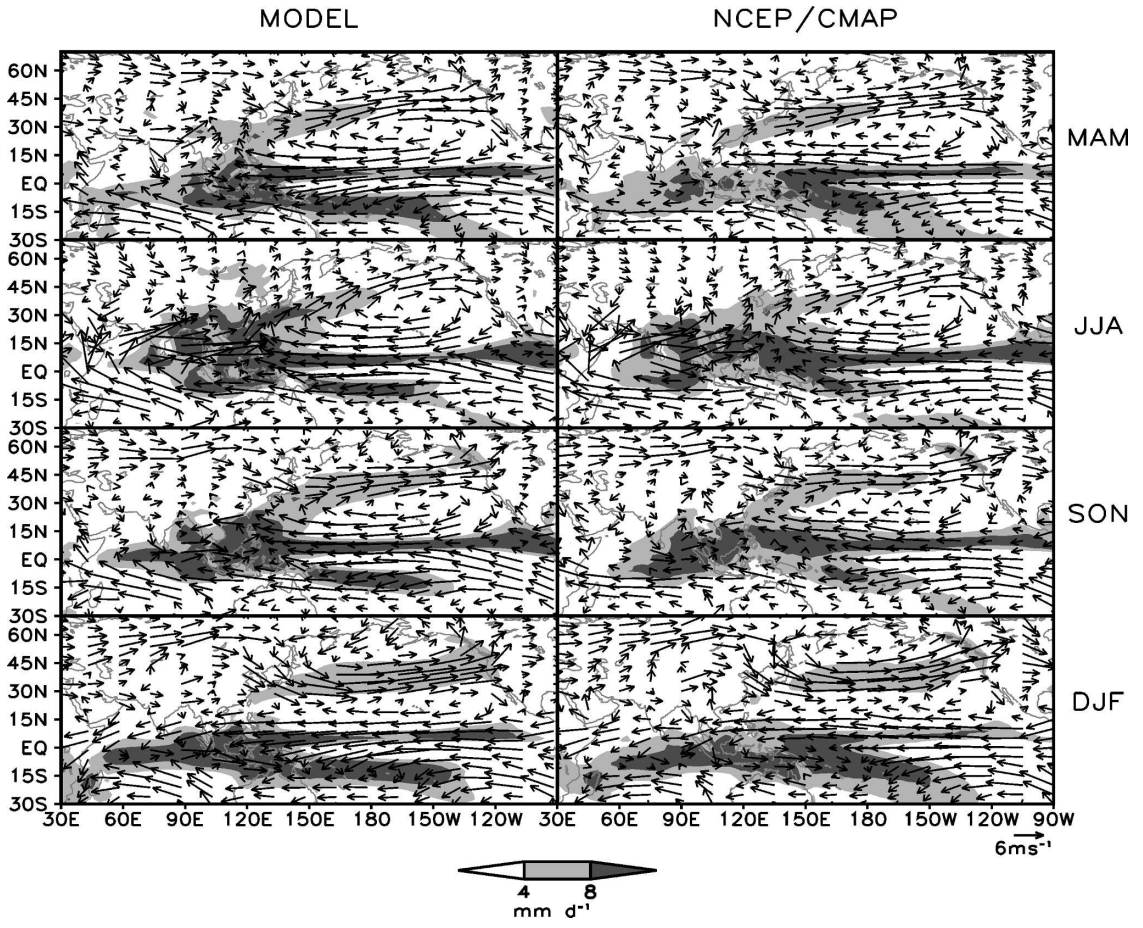

FIG. 1. Climatological distribution of the 850-hPa horizontal winds (vector) and precipitations (shading, see scale bar at bottom) for the four seasons in the (left) simulation and (right) observations, averaged over 1000 yr for the simulation and 25 yr (1979–2003) for observations. Unit is in mm day^{-1} for precipitations and m s^{-1} for winds.

ship, although this relationship has been well documented in many previous observational studies. For observations, the El Niño events are 1957–58, 1965–66, 1969–70, 1972–73, 1976–77, 1982–83, 1987–88, 1991–92, and 1997–98 (9 events) and the La Niña events are 1950–51, 1954–55, 1955–56, 1964–65, 1970–71, 1973–74, 1975–76, 1988–89, and 1998–99 (9 events). These chosen ENSO events are identical to those in Lau and Nath (2000) and Alexander et al. (2002), who followed the ENSO definition of Trenberth (1997).

a. SST anomalies

Figure 2 shows the composite time evolution of the Niño-3 index for the El Niño and La Niña events, respectively. The time window spanning 4 yr is centered in the ENSO mature phase of D(0)JF(1). For the El Niño events, the composite evolution in the simulation coincides well with that in observations. The model basically reproduces the amplitude and growth/decay of

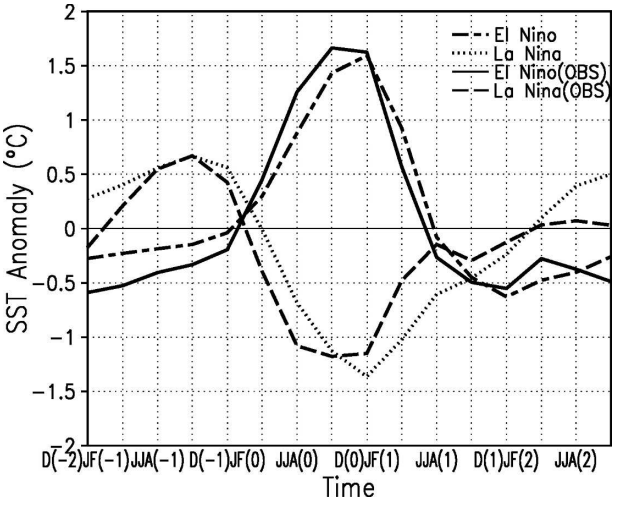

FIG. 2. Composite evolution of the Niño-3 index for El Niño (long dashed and short dashed), La Niña (dotted) in the simulation, and El Niño (solid), La Niña (dashed) in observations.

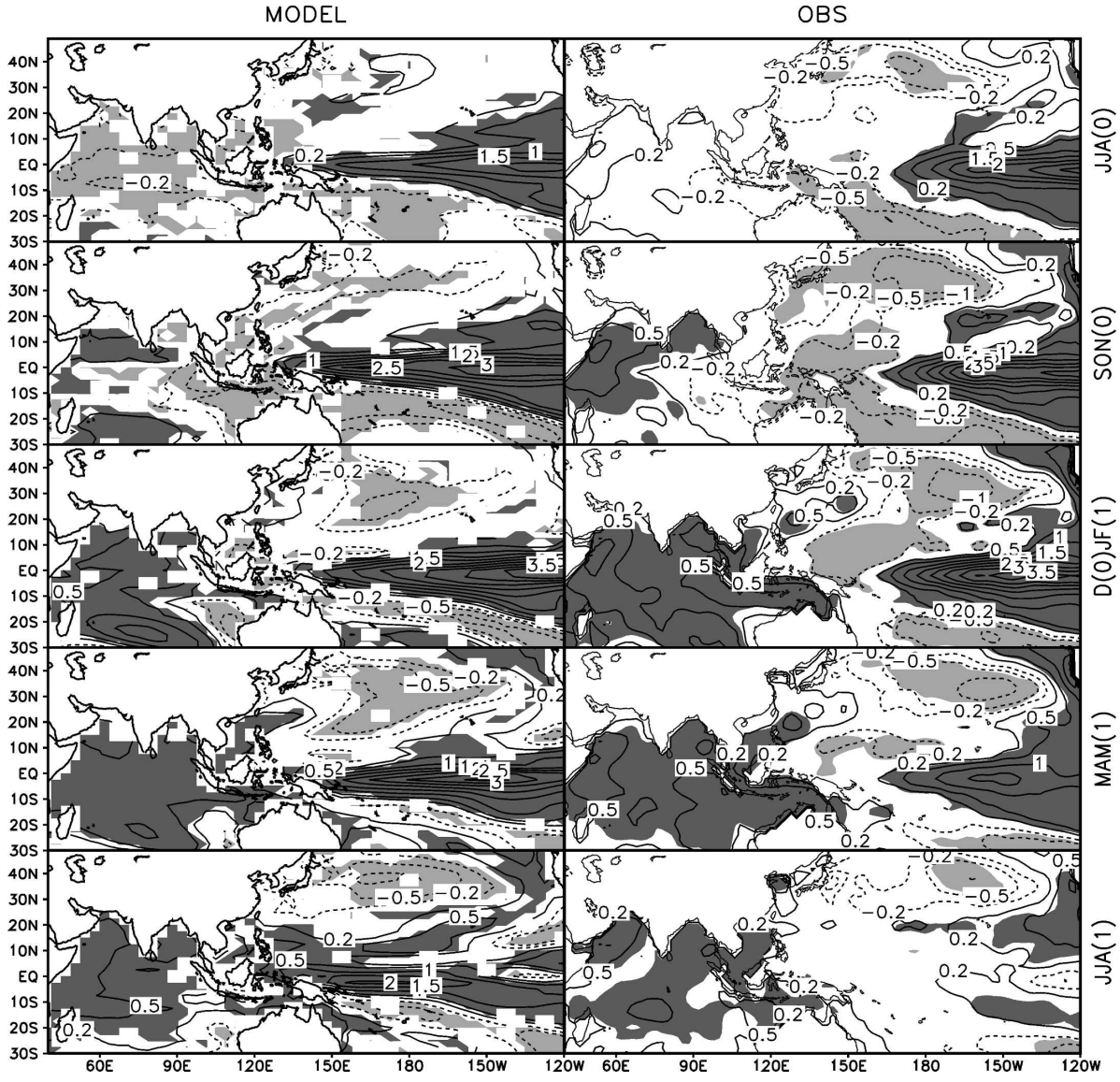

FIG. 3. Warm-minus-cold composites of SSTs for the (left) simulation and (right) observations from JJA(0) to JJA(1). Unit is °C; contour interval is 0.5, with additional contours −0.2 and +0.2 inserted. The shadings indicate the regions of 99% confidence level by using a lookup table test for the simulation and 95% confidence level by using a two-tailed Student's *t* test for observations.

El Niño events and also captures the times of transitions between positive and negative phases. A discrepancy appears in (July–August) JJA(0) and (September–November) SON(0), when the simulated Niño-3 index is smaller than the observed. As for the La Niña events, the model simulates a delayed phase in comparison with observations. Particularly, the La Niña events exhibit a prolonged decaying process in the simulation with some discrepancies appearing in JJA(1) and SON(1).

We perform composite analyses based on the warm and cold events and show the results of composite differences for five consecutive seasons from JJA(0) to JJA(1) to illustrate the evolution of SST and circulation anomalies associated with the different phases of ENSO. The statistical significance is determined by using a two-tailed Student's *t* test for observations and lookup table test for the simulation. The lookup table test can avoid the difficulties of estimating an equivalent sample size (von Storch and Zwiers 1999). Figure 3 shows the composite differences of SSTs. In observations, there are positive SST anomalies in the eastern equatorial Pacific in JJA(0). The magnitude of these anomalies subsequently grows over the next two sea-

sons, reaches a peak in D(0)JF(1), weakens in (March–May) MAM(1), and returns to a normal state in JJA(1). In the western North Pacific, there are negative SST anomalies from SON(0) to MAM(1) with an amplitude of about 0.2°C. In the Indian Ocean, SST anomalies with a dipolelike distribution in SON(0) become positive in the whole basin in the subsequent three seasons [from D(0)JF(1) to JJA(1)]. These features are consistent with those shown in Nigam and Shen (1993) and Wang et al. (2003) based on observations.

These observed patterns of anomalous SSTs in the tropical Pacific and Indian Oceans are well reproduced by the model. The model well simulates the evolution of the positive SST anomalies in the tropical eastern Pacific and the transition from a dipolelike anomalous SST pattern in SON(0) to basinwide positive anomalies in MAM(1) and JJA(1) in the Indian Ocean. However, the simulated SST warming in the tropical eastern Pacific extends farther westward than is observed, likely to be associated with the typical error of model climatology of the cold tongue and associated shallow thermocline in this region (Collins et al. 2001). This is a common problem experienced by many global coupled models (e.g., Latif et al. 2001; Meehl et al. 2001). In addition, the model simulates cold SSTs in the subtropical southeast Indian Ocean in D(0)JF(1). This in turn leads to a delayed warming of the whole Indian Ocean. In addition, the inaccuracy of the model-simulated dipole variability in the Indian Ocean may also play a role. Spencer et al. (2005) indicated that the Indian Ocean dipole pattern in the model persists through the boreal winter and into the following year due to the lack of negative feedback while, in nature, the dipole pattern terminates in the boreal winter.

b. Evolution of the anomalous anticyclone in the western North Pacific

The circulation anomalies over the WNP are dominated by the anomalous anticyclone, which is noted by Wang et al. (2003) as one of the El Niño–associated off-equatorial anomalous anticyclones in the Asian monsoon region. In both observations and the model simulation, westerly anomalies extend from the South China Sea eastward into the central and eastern Pacific and a weak anomalous anticyclone appears over the Bay of Bengal in JJA(0) (Fig. 4). This anticyclonic anomaly expands and occupies a broad region extending from the Arabian Sea eastward to the South China Sea in SON(0). It shifts eastward in D(0)JF(1) and appears over the WNP in the subsequent spring. In JJA(1), this anticyclonic anomaly weakens dramatically and there is a weak easterly anomaly in the equatorial western Pacific. The transition from the westerly anomaly in JJA(0) to the easterly anomaly in JJA(1) implies that a TBO signal in the western Pacific is associated with the ENSO. Associated with the anomalous WNP anticyclone in MAM(1) is a dipole pattern of local SST anomalies with cold and warm anomalies to the east and west, respectively (Fig. 3), which has been mentioned by Wang et al. (2000).

The evolution of the WNP anticyclonic anomaly is associated with precipitation anomalies (not shown). It is found that, both in observations and the simulation, precipitation is significantly suppressed over the Maritime Continent and eastern Indian Ocean in JJA(0) and SON(0), and the negative precipitation anomaly shifts eastward into the South China Sea and the Philippine Sea in MAM(1).

c. Evolution of the anomalous anticyclone in the south Indian Ocean

The off-equatorial anomalous anticyclone over the south Indian Ocean is another important feature of the interannual Asian–Australian variability associated with the ENSO events (Wang et al. 2003). The model reproduces well the observed evolution of the SIO anticyclonic anomaly (Fig. 4). In both observations and the simulation, a weak anticyclonic anomaly appears over the SIO in JJA(0), rapidly reaches its peak intensity in SON(0), retreats eastward in D(0)JF(1), and weakens in MAM(1). The SIO anomalous anticyclone during the period of peak intensity is associated with the dipole pattern of SST anomalies (Fig. 3) (Wang et al. 2003). Although the model fails to simulate accurately the evolution of the Indian Ocean dipole pattern (Spencer et al. 2005), this discrepancy seems not to noticeably affect the evolution of the SIO anomalous anticyclone associated with the phases of ENSO.

4. WNP/SIO anomalous anticyclones and ENSO phase transition

In this section, we investigate the relationship between the transition of the ENSO phases and the evolution of the WNP/SIO anomalous anticyclones in the simulation, considering strong and moderate ENSO events separately. The reasonable reproduction of the evolution of these anticyclonic anomalies associated with the ENSO cycle shown in the previous section provides a prerequisite for the analysis in this section. In this sense, we analyze the evolution associated with the El Niño events in order to minimize the possible effects of the model's bias toward slower than normal decay for La Niña events. We divide the total 152 El Niño events in the 1000-yr simulation into two catego-

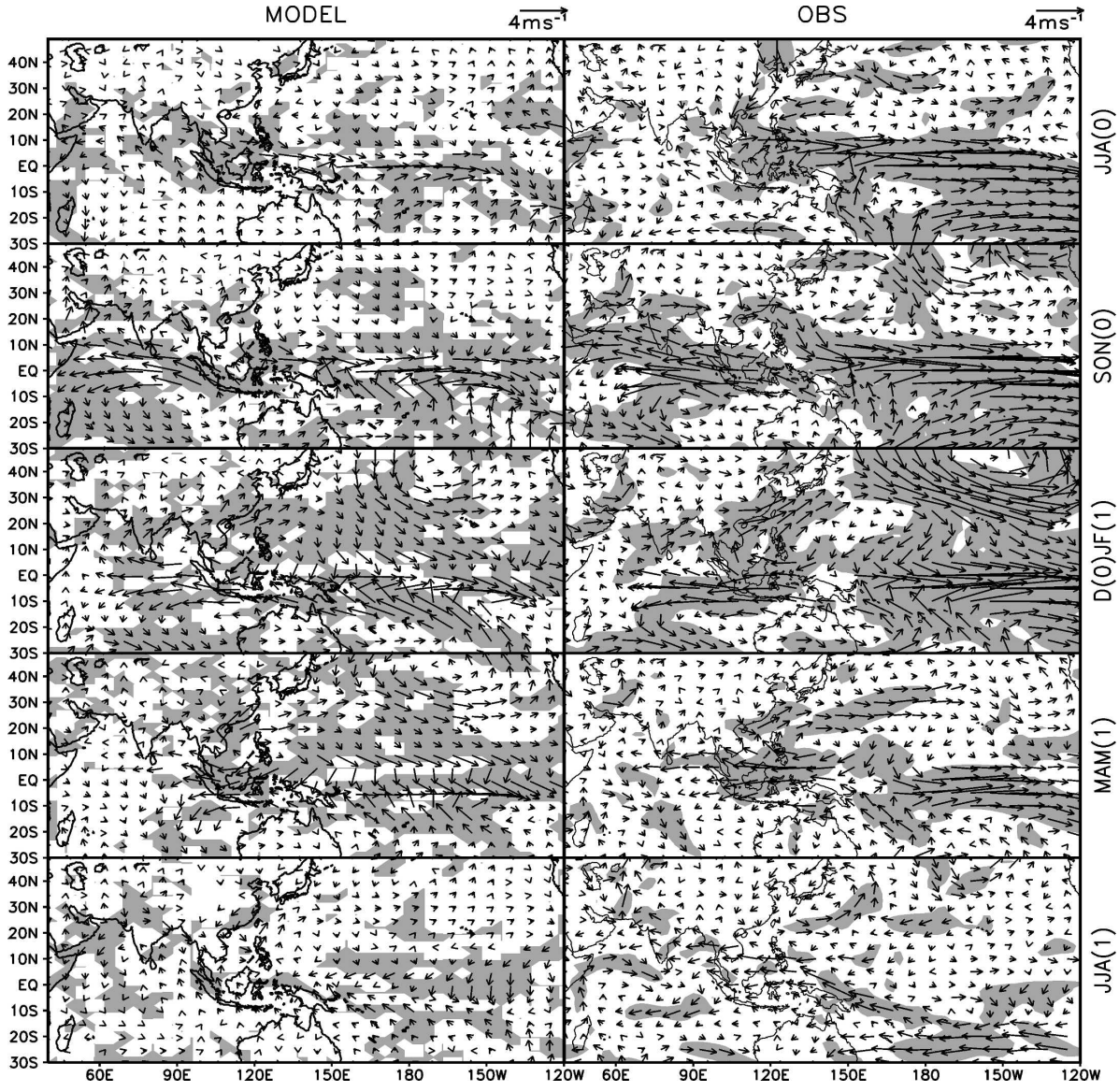

FIG. 4. As in Fig. 3, but for 850-hPa winds: shading indicates the regions of confidence level for either zonal or meridional wind.

ries: strong and moderate events. The events with the Niño-3 index averaged in winter being greater than 1.5 standard deviations from the time mean are classified as strong events and the rest as moderate events. This criterion yields 70 strong events and 82 moderate events. Figure 5 depicts the evolution of the Niño-3 index for the composite strong and moderate El Niño events, respectively. The growing phase of composite strong El Niño events is similar to that of composite moderate ones. However, the strong El Niño events tend to be followed by a much more rapid decay, while the moderate El Niño events are followed by a slower decay. In fact, 39 (56%) of 70 strong El Niño events, but only 19 (23%) of 82 moderate El Niño events, become La Niña events in the subsequent winter. This indicates that strong El Niño events are more likely to turn into La Niña events in the subsequent winter and thus favor the ENSO biennial cycle. Such a tendency can also be noticed in previous observational results (Boo et al. 2004; Kug and Kang 2006), although limited cases in observations preclude any solid conclusions on the relationship between the intensity and the tendency for ENSO transition to occur.

Figure 6 shows the seasonal sequence of composite 850-hPa streamfunction anomalies associated with the strong and moderate El Niño events, respectively. We expand three consecutive seasons after JJA(1) to illustrate the feature of biennial oscillation. During JJA(0)–

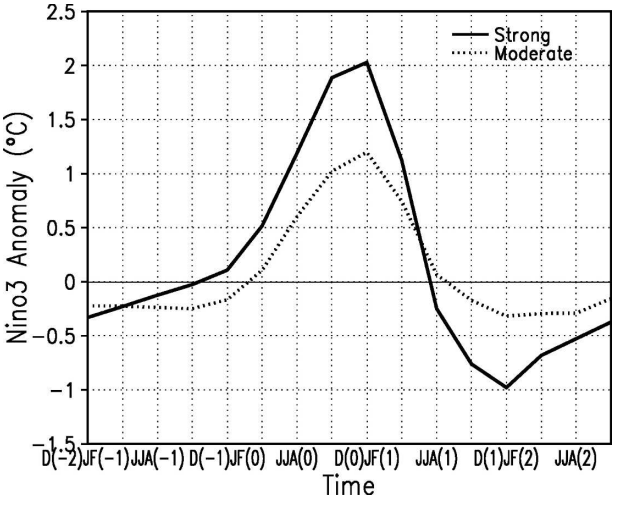

FIG. 5. Composite evolution of the Niño-3 index for the strong (solid) and moderate (dotted) El Niño events.

MAM(1), the evolution of streamfunction anomalies, both for strong and moderate events, is consistent with that of horizontal wind anomalies shown in the left panels of Fig. 4, but Fig. 6 shows more clearly the changes in the SIO/WNP anomalous anticyclones. The streamfunction anomalies are significantly greater for strong cases than for moderate cases, not only over the central and eastern Pacific where it is expected but also over the Asian monsoon region, which suggests that the strong events are associated with stronger interaction with the Asian monsoon.

From JJA(1), the streamfunction anomalies exhibit a remarkable difference between the strong and moderate cases. For the strong cases, there are twin anticyclonic anomalies in the western and central Pacific located north and south of the equator, respectively. These twin anticyclonic anomalies over the western and central Pacific shift eastward in the subsequent seasons and reach the eastern Pacific in MAM(2). In the Indian Ocean, a pair of cyclonic anomalies is initiated in SON(1) and moves to around 120°E in MAM(2). Comparison of the evolution between the first four seasons [JJA(0) to MAM(1)] and the following four seasons [JJA(1) to MAM(2)] reveals that the streamfunction anomalies have nearly reversed polarities in the Indian and Pacific Oceans between these two periods, indicating that strong El Niño events are associated with a strong biennial tendency of low-level circulation variability. In contrast, for moderate cases, there are almost no significant anomalies in the seasons since JJA(1), and thus the biennial tendency does not exist. This result suggests that the pair of anticyclonic anomalies in the western and central Pacific in JJA(1) might play a crucial role in the transition from strong El Niño events to La Niña events in the subsequent winter.

Figure 7 shows a clearer biennial cycle of the SIO/WNP anomalous anticyclones in the strong cases, but not in the moderate cases. The SIO anticyclonic anomaly, which attains its maximum in SON(0), becomes a cyclonic anomaly in SON(1) in the strong cases, but persists in the moderate cases. The WNP anticyclonic anomaly in D(0)JF(1) and MAM(1) also shows a clear transition into a cyclonic anomaly in D(1)JF(2) and MAM(2) in the strong cases, but does not in the moderate cases. In addition, there is a clear difference in the WNP circulation anomaly in JJA(1) between the strong and moderate composites: an anticyclonic anomaly in the strong cases but a weak cyclonic anomaly in the moderate cases.

It has been shown that the WNP anticyclonic anomaly in MAM(1) is closely related to the SIO anticyclonic anomaly in SON(0) through the ENSO cycle, with the former being the result of an eastward shift of the latter (Figs. 4 and 6). Figure 8 is presented to further illustrate the relationship between these two anticyclonic anomalies. Without the effects of ENSO events in D(0)JF(1), a SIO anticyclonic anomaly in SON(0) does not correspond to a WNP anticyclonic anomaly in MAM(1) (Fig. 8a), also indicated by a small R-squared value of 0.01. When there are ENSO events occurring in D(0)JF(1), the relationship between these two anticyclonic anomalies becomes enhanced significantly (Figs. 8b and 8c). The R-squared values for the moderate and strong ENSO events are 0.23 and 0.48, respectively. Particularly for the strong events, the linear regression between the SIO and WNP anticyclonic anomalies explains nearly half of the variance.

We further classify the strong El Niño events into two categories according to whether or not they are followed by La Niña events in the subsequent winter. We then examine the evolution of the composite 850-hPa streamfunction and SST anomalies for these two categories, respectively. As mentioned previously, there are 39 strong El Niño events followed by and 31 events not followed by La Niña events in the subsequent winter [D(1)JF(2)]. Hereafter, these 39 cases and 31 cases are referred to as category A and category B, respectively. From JJA(0) to MAM(1), the composite anomalies of both 850-hPa streamfunction and SST show a good deal of resemblance between the two categories (not shown). A clear distinguished feature of the composite anomalies between the two categories appears in JJA(1) (Fig. 9). Twin anticyclonic anomalies appear in the western and central Pacific for category A, but they are much weakened for category B (Figs. 9a and 9b). In comparison with the streamfunction anoma-

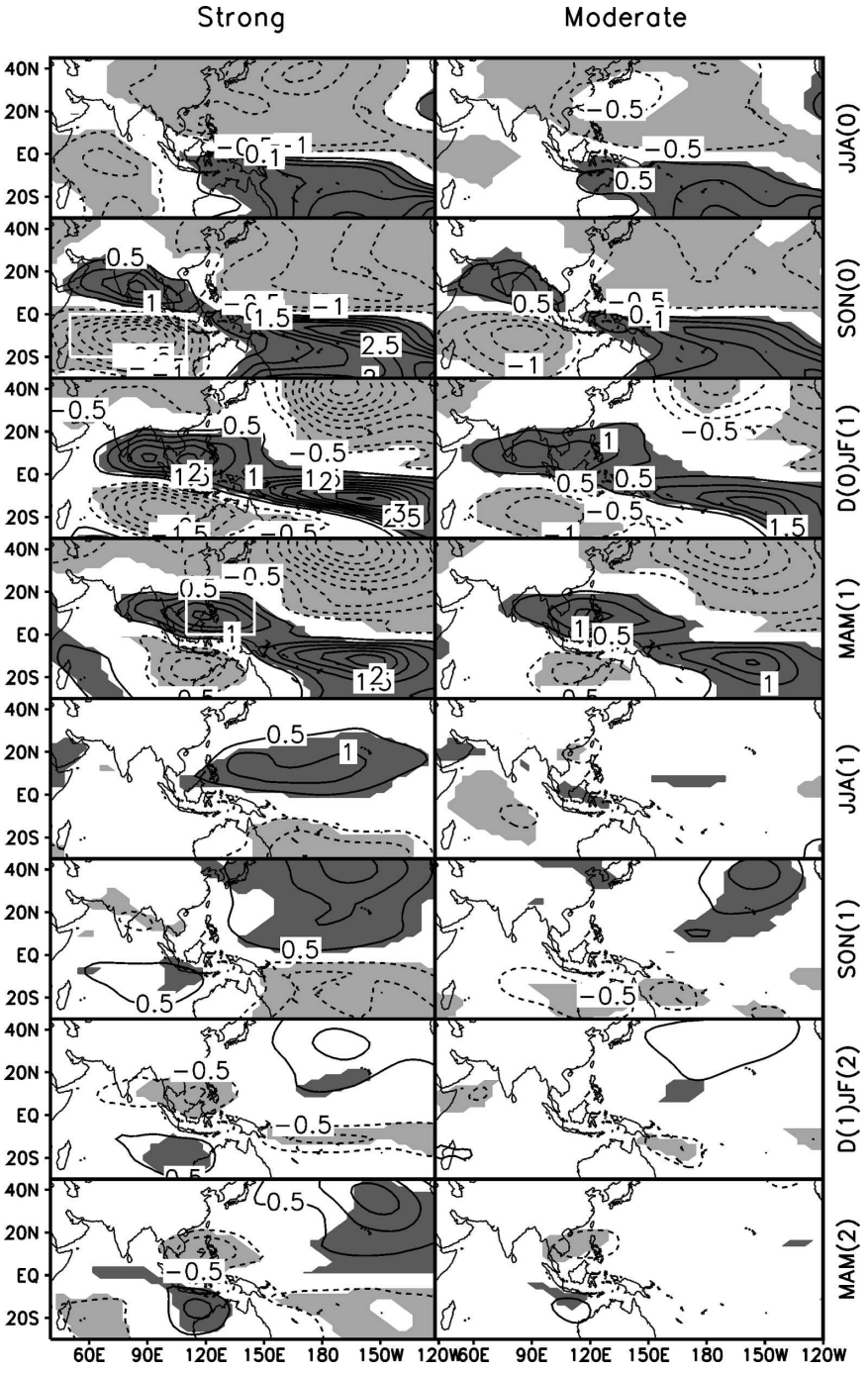

FIG. 6. Composite 850-hPa streamfunction anomalies for (left) strong and (right) moderate El Niño events at the eight stages of the ENSO cycle. Unit is 10^6 m^2 s^{-1}. The contour interval is 0.5; shading indicates the regions of 99% confidence level by using the lookup table test. Boxed areas in the left panels show the averaging areas for the south Indian Ocean and western North Pacific in Fig. 7.

lies, the SST anomalies show a much weaker distinction between the two categories (Figs. 9c and 9d). In particular, the SST anomalies are almost indistinguishable from each other in the Indian Ocean and the western Pacific between the two categories. The negative SST anomalies in the equatorial eastern Pacific are stronger to some extent for category A than for category B. From SON(1) to MAM(2), the SST anomalies exhibit a

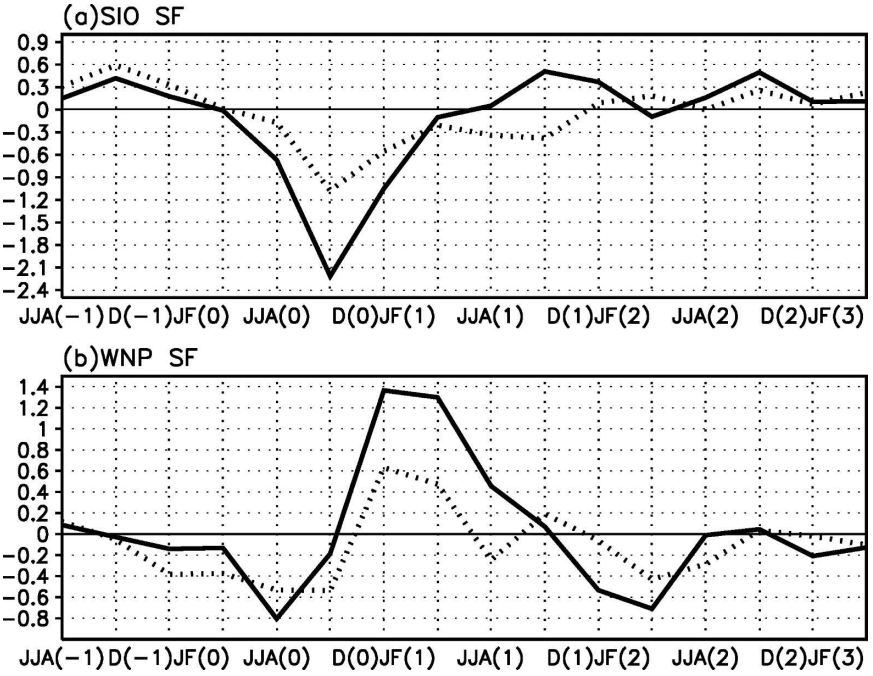

FIG. 7. Composite evolution of 850-hPa streamfunction anomalies (unit: 10^6 m^2 s^{-1}) averaged over the (a) SIO (20°S–0°, 50°–110°E) and (b) WNP (0°–25°N, 110°–145°E), for the strong (solid line) and moderate (dotted line) El Niño events.

La Niña pattern in the Pacific and Indian Oceans for category A but are extremely weak for category B (not shown). This result further demonstrates that the pair of anticyclonic anomalies in the western and central Pacific in JJA(1) plays a crucial role in the 1-yr duration of the phase transition of ENSO.

This pair of anticyclonic anomalies in the western and central Pacific plays an important role in terminating El Niño events and in triggering La Niña events through the easterly anomaly at the equator (Weisberg and Wang 1997; Wang et al. 1999). In terms of causing the zonal wind anomalies over the equatorial western Pacific, some studies emphasize the effect of local SST anomalies (Weisberg and Wang 1997; Wang et al. 1999; Wang et al. 2000), while some other studies suggest that the Indian Ocean SST variability plays an important role (Watanabe and Jin 2002; Terao and Kubota 2005; Annamalai et al. 2005; Kug and Kang 2006). In particular, Kug and Kang suggest that an easterly wind anomaly over the western Pacific induced by the warming in the Indian Ocean during the mature phase of El Niño helps bring about a rapid termination of El Niño and a fast transition to La Niña. In our results, however, from the mature phase of El Niño to the subsequent summer, the SST anomalies in the Indian Ocean and the western Pacific do not show a clear distinction between the two categories. Therefore, the previously proposed mechanism that the zonal wind anomalies over the western Pacific result from the local and remote anomalous SSTs, proposed by the previous studies, cannot be used to explain the distinction between circulation anomalies in the two categories, or the appearance of the pair of anomalous anticyclones over the western and central Pacific in JJA(1) in our results.

Figure 10 shows the composite anomalies of 200-hPa zonal winds in JJA(1) for the two categories, respectively. Zonally oriented cells of anomalies with alternating signs extend from northeastern Asia southward into the western South Pacific for category A (Fig. 10a). These cells resemble a teleconnection pattern over the western and central Pacific, suggesting a link between the tropical and extratropical circulation anomalies. The easterly anomaly over northeastern Asia and the westerly anomaly over the subtropical western North Pacific indicate a southward displacement of the East Asian upper-tropospheric westerly jet (EAJ), the axis of which is located at about 40°N in summer. The EAJ is an integrated component of the East Asian summer monsoon system, and a southward displacement of the EAJ corresponds to enhanced precipitations along the monsoonal rainy belt (Lau et al. 2000; Lu 2004). In the simulation, there is significantly enhanced precipitation in East Asia and the subtropical western North Pacific for category A (not shown). A southward displacement

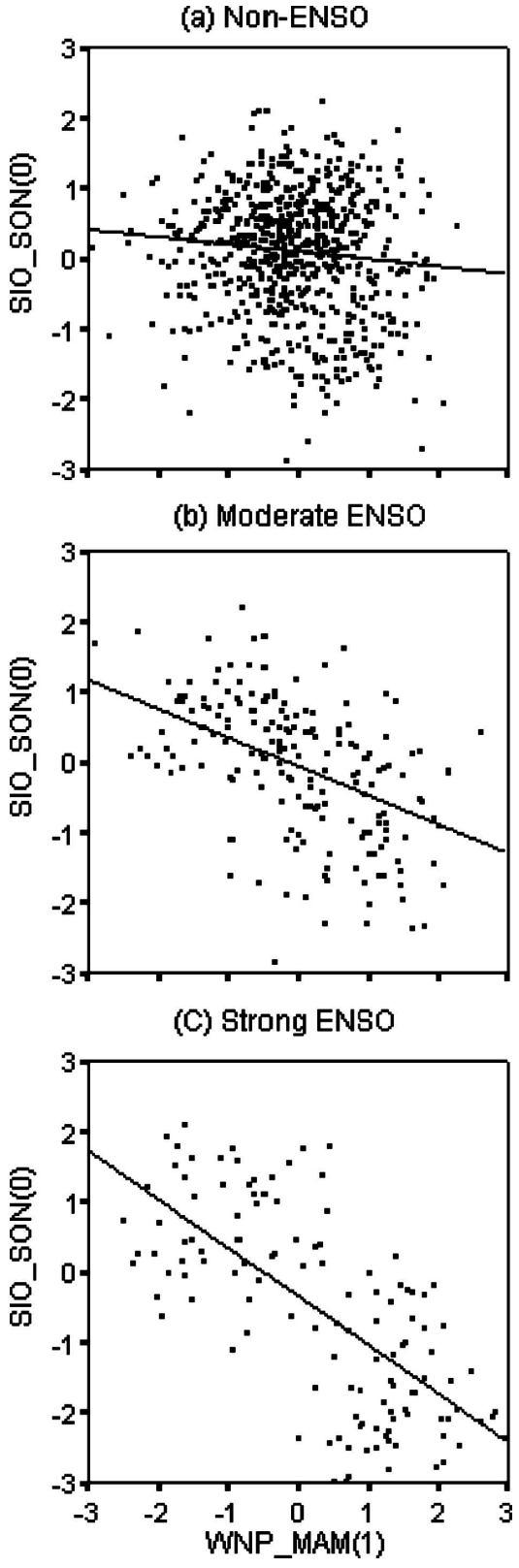

FIG. 8. Scatter diagrams of 850-hPa streamfunction anomalies averaged over the SIO (20S°–0°, 50°–110°E) in SON(0) and over the WNP (0°–25°N, 110°–145°E) in MAM(1): (a) non-ENSO cases; (b) moderate ENSO events; and (c) strong ENSO events.

of the EAJ corresponds to the cooler SSTs in the equatorial eastern Pacific in observations (Lu 2005). However, the meridional displacement of the EAJ is dominated by the internal atmospheric variability (Lu et al. 2006). For category B, the teleconnection pattern is weakened (Fig. 10b), and there is no significantly enhanced precipitation in East Asia and the subtropical western North Pacific (not shown). These results suggest that the East Asian summer monsoon, which is influenced by the ENSO, can in turn affect ENSO.

5. Summary

Both the ENSO and Asian monsoon and the coupling between them are prominent representatives of coupled ocean–atmosphere interactions, contributing considerably to climate variability in many parts of the world. Therefore, evaluating the ENSO–Asian monsoon interaction can be an important test for coupled models. In this paper, we have evaluated this interaction in an atmosphere–ocean fully coupled GCM (HadCM3). The evaluation is focused on the two evolving anomalous anticyclones: one located over the WNP and the other over the SIO, which was found to be crucial in linking the Asian monsoon to the ENSO in observations (Wang et al. 2003). Using such an evaluation as a basis, we have examined the relationship between the WNP/SIO anomalous anticyclones and ENSO cycle, using the adequately long period of the HadCM3 simulation.

The coupled model captures well the observed features of the evolution of WNP and SIO anomalous anticyclones and SSTs associated with the ENSO cycle. As in observations, the WNP anticyclone in the simulation forms in the autumn of a growing El Niño [SON(0)], reaches its peak intensity during the El Niño mature winter [D(0)JF(1)] and the following spring [MAM(1)], and decays rapidly in the subsequent summer [JJA(1)]. On the other hand, the SIO anticyclone in the model forms during the summer of El Niño development, attains maximum intensity in the subsequent autumn, and decays during the following two seasons. The cold and warm SST anomalies to the east and west of the anomalous WNP anticyclone in D(0)JF(1) and MAM(1) are also captured. In the Indian Ocean, the dipole pattern of SST anomalies in SON(0) and basinwide positive SST anomalies from D(0)JF(1) to MAM(1) are basically simulated.

We then examined the ENSO–monsoon interaction in the model since the 1000-yr simulation provides an adequate sample size of the ENSO cycle and thus makes statistical analyses possible. First, we found that the strong El Niño events, defined by a DJF Niño-3

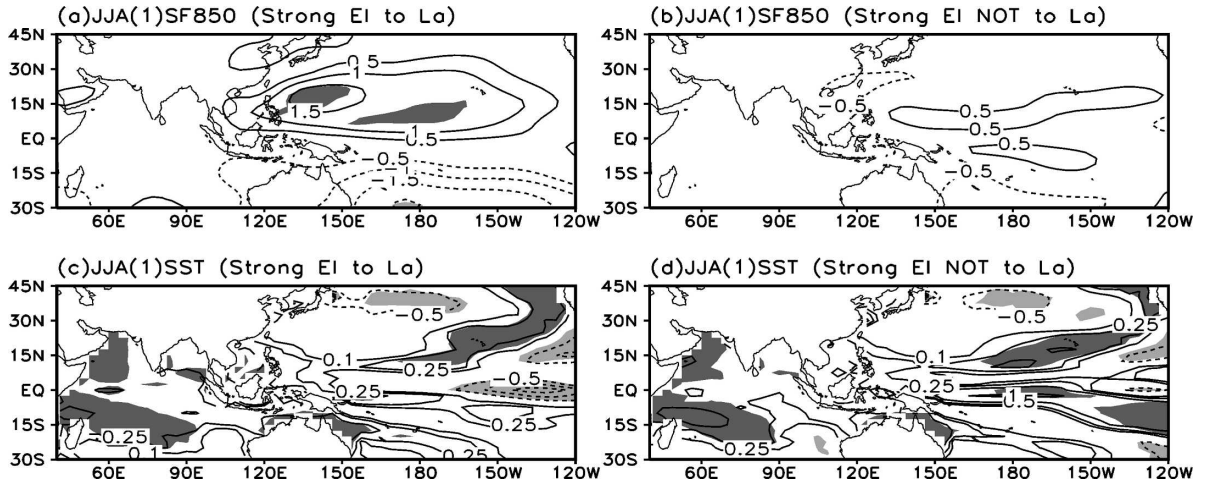

FIG. 9. Composite anomalies of (a), (b) 850-hPa streamfunction (unit: 10^6 m^2 s^{-1}) and (c), (d) SST (unit: °C) in JJA(1) for the cases of strong El Niño events in D(0)JF(1) (a), (c) followed by and (b), (d) not followed by La Niña events in D(1)JF(2). Shading indicates the regions of 95% confidence level by using a Student's *t* test. For the SST anomalies, additional contours of 0.1 and 0.25 are inserted to show the details in the Indian Ocean and western Pacific.

index being greater than 1.5 standard deviations from the mean in this study, have a greater possibility of being followed by La Niña events one year later.

We found that the twin anomalous anticyclones north and south of the equator in the western Pacific in the summer of the decaying El Niño are crucial for this 1-yr transition from El Niño to La Niña. The appearance of these anticyclonic anomalies is favored by the strong El Niño events in the preceding winter, but it seems not to be related with simultaneous SST anomalies in the Indian Ocean and western Pacific. The variability in the East Asian summer monsoon seems to be responsible for the appearance of the WNP anticyclonic anomaly through an upper-tropospheric meridional teleconnection pattern over the western and central Pacific. This study suggests that the TBO tendency of the SIO and WNP anticyclonic (cyclonic) anomalies is intimately related to the ENSO and that both ENSO and the SIO/WNP circulation anomalies are tied to the TBO. In addition, the ENSO events, especially those strong ones, enhance significantly the correspondence between the SIO anticyclonic (cyclonic) anomaly in the preceding autumn and WNP anticyclonic (cyclonic) anomaly in the subsequent spring. This correspondence explains nearly half of the variance for the strong ENSO cases but only 1% of the variance for the non-ENSO cases.

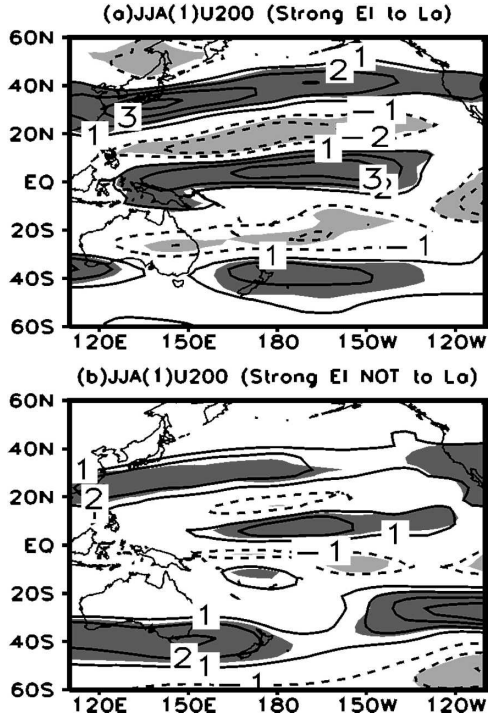

FIG. 10. Composite anomalies of 200-hPa zonal winds (unit: m s^{-1}) in JJA(1) for the cases of strong El Niño events in D(0)JF(1) (a) followed by and (b) not followed by La Niña events in D(1)JF(2).

In this study we have focused on the relationship between the ENSO and basinwide circulation anomalies, which are characterized by the SIO and WNP anticyclonic anomalies, but we did not examine the features of the ENSO–monsoon interaction in regional details. In addition, we did not show the results for the boreal autumn of La Niña decay and the subsequent seasons, due to the overly prolonged La Niña decaying phases in the simulation. This is the most serious bias

affecting the evaluation of the ENSO–Asian monsoon interaction. In addition, since the present results might be model specific, further studies with other coupled models as well as observations are required.

Acknowledgments. This work is supported by the National Natural Science Foundation of China (Grant 40475025). Buwen Dong is supported by the ENSEMBLES Project (GOCE-CT-2003-505539) at the National Centre for Atmospheric Science-Climate. The comments of Dr. Sumant Nigam and two anonymous reviewers led to great improvement of this paper. We are grateful to colleagues at the Met Office Hadley Centre for providing the model simulation and Mark A. Miller at Princeton University for carefully revising the manuscript.

REFERENCES

AchutaRao, K., and K. Sperber, 2002: Simulation of the El Niño Southern Oscillation: Results from the Coupled Model Intercomparison Project. *Climate Dyn.,* **19,** 191–209.

Alexander, M. A., I. Blade, M. Newman, J. R. Lanzante, N.-C. Lau, and J. D. Scott, 2002: The atmospheric bridge: The influence of ENSO teleconnections on air–sea interaction over the global oceans. *J. Climate,* **15,** 2205–2231.

Annamalai, H., P. Liu, and S.-P. Xie, 2005: Southwest Indian Ocean SST variability: Its local effect and remote influence on Asian monsoons. *J. Climate,* **18,** 4150–4167.

Barnett, T. P., 1991: The interaction of multiple time scales in the tropical climate system. *J. Climate,* **4,** 269–285.

Boo, K.-O., G.-H. Lim, and K.-Y. Kim, 2004: On the low-level circulation over the western North Pacific in relation with the duration of El Niño. *Geophys. Res. Lett.,* **31,** L10202, doi:10.1029/2004GL019418.

Chang, C.-P., Y. Zhang, and T. Li, 2000: Interannual and interdecadal variations of the East Asian summer monsoon and tropical Pacific SSTs. Part I: Roles of the subtropical ridge. *J. Climate,* **13,** 4310–4325.

Chou, C., J.-Y. Tu, and J.-Y. Yu, 2003: Interannual variability of the western North Pacific summer monsoon: Differences between ENSO and non-ENSO years. *J. Climate,* **16,** 2275–2287.

Chung, C., and S. Nigam, 1999: Asian summer monsoon—ENSO feedback on the Cane–Zebiak model ENSO. *J. Climate,* **12,** 2787–2807.

Collins, M., S. F. B. Tett, and C. Cooper, 2001: The internal climate variability of HadCM3, a version of the Hadley Centre coupled model without flux adjustments. *Climate Dyn.,* **17,** 61–81.

Elliot, W. P., and J. K. Angell, 1987: The relation between Indian monsoon rainfall, the Southern Oscillation, and hemispheric air and sea temperature: 1884–1984. *J. Climate Appl. Meteor.,* **26,** 943–948.

Gordon, C., C. Cooper, C. A. Senior, H. Banks, J. M. Gregory, T. C. Johns, F. B. Mitchell, and R. A. Wood, 2000: The simulation of SST, sea ice extents and ocean heat transports in a version of the Hadley Centre coupled model without flux adjustments. *Climate Dyn.,* **16,** 147–168.

Guilyardi, E., 2006: El Niño mean state seasonal cycle interactions in a multi-model ensemble. *Climate Dyn.,* **26,** 329–348.

Joseph, R., and S. Nigam, 2006: ENSO evolution and teleconnections in IPCC's twentieth-century climate simulations: Realistic representation? *J. Climate,* **19,** 4360–4377.

Kalnay, E., and Coauthors, 1996: The NCEP/NCAR 40-Year Reanalysis Project. *Bull. Amer. Meteor. Soc.,* **77,** 437–471.

Kim, K.-M., and K.-M. Lau, 2001: Dynamics of monsoon-induced biennial variability in ENSO. *Geophys. Res. Lett.,* **28,** 315–318.

Kirtman, B. P., and J. Shukla, 2002: Interactive coupled ensemble: A new coupling strategy for CGCMs. *Geophys. Res. Lett.,* **29,** 1367, doi:10.1029/2002GL014834.

Kug, J.-S., and I.-S. Kang, 2006: Interactive feedback between ENSO and the Indian Ocean. *J. Climate,* **19,** 1784–1801.

Latif, M., and Coauthors, 2001: ENSIP: The El Niño simulation intercomparison project. *Climate Dyn.,* **18,** 255–276.

Lau, K.-M., K.-M. Kim, and S. Yang, 2000: Dynamical and boundary forcing characteristics of regional components of the Asian summer monsoon. *J. Climate,* **13,** 2461–2482.

Lau, N.-C., and M. J. Nath, 2000: Impact of ENSO on the variability of the Asian–Australian monsoons as simulated in GCM experiments. *J. Climate,* **13,** 4287–4309.

Li, T., P. Liu, X. Fu, B. Wang, and G. A. Meehl, 2006: Spatiotemporal structures and mechanisms of the tropospheric biennial oscillation in the Indo–Pacific warm ocean regions. *J. Climate,* **19,** 3070–3087.

Lu, R., 2002: Precursory SST anomalies associated with the convection over the western Pacific warm pool. *Chin. Sci. Bull.,* **47,** 696–699.

——, 2004: Associations among the components of the East Asian summer monsoon system in the meridional direction. *J. Meteor. Soc. Japan,* **82,** 155–165.

——, 2005: Interannual variation of North China rainfall in rainy season and SSTs in the equatorial eastern Pacific. *Chin. Sci. Bull.,* **50,** 2069–2073.

——, Y. Li, and B. Dong, 2006: External and internal summer atmospheric variability in the western North Pacific and East Asia. *J. Meteor. Soc. Japan,* **84,** 447–462.

Mechoso, C. R., and Coauthors, 1995: The seasonal cycle over the tropical Pacific in coupled ocean–atmosphere general circulation models. *Mon. Wea. Rev.,* **123,** 2825–2838.

Meehl, G. A., 1994: Coupled land–ocean–atmosphere processes and south Asian monsoon variability. *Science,* **266,** 263–267.

——, 1997: The south Asian monsoon and the tropospheric biennial oscillation. *J. Climate,* **10,** 1921–1943.

——, P. Gent, J. M. Arblaster, B. Otto-Bliesner, E. Brady, and A. Craig, 2001: Factors that affect amplitude of El Niño in global coupled climate models. *Climate Dyn.,* **17,** 515–526.

Nigam, S., and H.-S. Shen, 1993: Structure of oceanic and atmospheric low-frequency variability over the tropical Pacific and Indian Oceans. Part I: COADS observations. *J. Climate,* **6,** 657–676.

Pope, V. D., M. L. Gallani, P. R. Rowntree, and R. A. Stratton, 2000: The impact of new physical parameterizations in the Hadley Centre climate model—HadAM3. *Climate Dyn.,* **16,** 123–146.

Prasad, K. D., and S. V. Singh, 1996: Forecasting the spatial variability of the Indian monsoon rainfall using canonical correlation. *Int. J. Climatol.,* **16,** 1379–1390.

Rasmusson, E. M., and T. H. Carpenter, 1982: Variations in tropical sea surface temperature and surface wind fields associated

with the Southern Oscillation/El Niño. *Mon. Wea. Rev.,* **110,** 354–384.

——, X. Wang, and C. F. Ropeleski, 1990: The biennial component of ENSO variability. *J. Mar. Syst.,* **1,** 71–96.

Shen, S., and K.-M. Lau, 1995: Biennial oscillation associated with the East Asian summer monsoon and tropical sea surface temperatures. *J. Meteor. Soc. Japan,* **73,** 105–124.

Shukla, J., and D. Paolino, 1983: The Southern Oscillation and the long-range forecasting of the summer monsoon rainfall over India. *Mon. Wea. Rev.,* **111,** 1830–1837.

Smith, T. M., and R. W. Reynolds, 2004: Improved extended reconstruction of SST (1854–1997). *J. Climate,* **17,** 2466–2477.

Spencer, H., R. T. Sutton, J. M. Slingo, M. Roberts, and E. Black, 2005: Indian Ocean climate and dipole variability in Hadley Centre coupled GCMs. *J. Climate,* **18,** 2286–2307.

Terao, T., and T. Kubota, 2005: East-west SST contrast over the tropical oceans and the post El Niño western North Pacific summer monsoon. *Geophys. Res. Lett.,* **32,** L15706, doi:10.1029/2005GL023010.

Trenberth, K. E., 1997: The definition of El Niño. *Bull. Amer. Meteor. Soc.,* **78,** 2771–2777.

Turner, A. G., P. M. Inness, and J. M. Slingo, 2005: The role of the basic state in the ENSO-monsoon relationship and implications for predictability. *Quart. J. Roy. Meteor. Soc.,* **131,** 781–804.

von Storch, H., and F. W. Zwiers, 1999: *Statistical Analysis in Climate Research*. Cambridge University Press, 484 pp.

Wang, B., and Q. Zhang, 2002: Pacific–East Asian teleconnection. Part II: How the Philippine Sea anomalous anticyclone is established during El Niño development. *J. Climate,* **15,** 3252–3265.

——, R. Wu, and X. Fu, 2000: Pacific–East Asian teleconnection: How does ENSO affect East Asian climate? *J. Climate,* **13,** 1517–1536.

——, ——, and K.-M. Lau, 2001: Interannual variability of the Asian summer monsoon: Contrasts between the Indian and the western North Pacific–East Asian monsoons. *J. Climate,* **14,** 4073–4090.

——, ——, and T. Li, 2003: Atmosphere–warm ocean interaction and its impacts on Asian–Australian monsoon variability. *J. Climate,* **16,** 1195–1211.

Wang, C., R. H. Weisberg, and J. I. Virmani, 1999: Western Pacific interannual variability associated with the El Niño-Southern Oscillation. *J. Geophys. Res.,* **104,** 5131–5149.

Watanabe, M., and F.-F. Jin, 2002: Role of Indian Ocean warming in the development of Philippine Sea anticyclone during ENSO. *Geophys. Res. Lett.,* **29,** 1478, doi:10.1029/2001GL014318.

Webster, P. J., and S. Yang, 1992: Monsoon and ENSO: Selectively interactive systems. *Quart. J. Roy. Meteor. Soc.,* **118,** 877–926.

Weisberg, R. H., and C. Wang, 1997: Slow variability in the equatorial west-central Pacific in relation to ENSO. *J. Climate,* **10,** 1998–2017.

Xie, P., and P. A. Arkin, 1997: Global precipitation: A 17-year monthly analysis based on gauge observations, satellite estimates, and numerical model outputs. *Bull. Amer. Meteor. Soc.,* **78,** 2539–2558.

Yasunari, T., 1990: Impact of the Indian monsoon on the coupled atmosphere ocean in the tropical Pacific. *Meteor. Atmos. Phys.,* **44,** 29–41.

Zhang, R., A. Sumi, and M. Kimoto, 1999: A diagnostic study of the impact of El Niño on the precipitation in China. *Adv. Atmos. Sci.,* **16,** 229–241.